

University of Nebraska - Lincoln DigitalCommons@University of Nebraska - Lincoln

Mechanical & Materials Engineering Faculty
Publications

Mechanical & Materials Engineering, Department
of

2019

Flaw detection with ultrasonic backscatter signal envelopes

Yongfeng Song

Central South University, songyf_ut@163.com

Christopher M. Kube

Penn State University, kube@psu.edu

Zuoxiang Peng

Southwest University, pzx@swu.edu.cn


Joseph A. Turner

University of Nebraska-Lincoln, jaturner@unl.edu

Xiongbing Li

Central South University, lixb_ex@163.com

Follow this and additional works at: <http://digitalcommons.unl.edu/mechengfacpub>

 Part of the [Mechanics of Materials Commons](#), [Nanoscience and Nanotechnology Commons](#), [Other Engineering Science and Materials Commons](#), and the [Other Mechanical Engineering Commons](#)

Song, Yongfeng; Kube, Christopher M.; Peng, Zuoxiang; Turner, Joseph A.; and Li, Xiongbing, "Flaw detection with ultrasonic backscatter signal envelopes" (2019). *Mechanical & Materials Engineering Faculty Publications*. 357.

<http://digitalcommons.unl.edu/mechengfacpub/357>

This Article is brought to you for free and open access by the Mechanical & Materials Engineering, Department of at DigitalCommons@University of Nebraska - Lincoln. It has been accepted for inclusion in Mechanical & Materials Engineering Faculty Publications by an authorized administrator of DigitalCommons@University of Nebraska - Lincoln.

Flaw detection with ultrasonic backscatter signal envelopes

Yongfeng Song,¹ Christopher M. Kube,² Zuoxiang Peng,³
 Joseph A. Turner,⁴ and Xiongbing Li^{1,a)}

¹*School of Traffic and Transportation Engineering, Central South University, Changsha, Hunan 410075, China*

²*Department of Engineering Science and Mechanics, Penn State University, University Park, Pennsylvania 16802, USA*

³*School of Mathematics and Statistics, Southwest University, Chongqing 400715, China*

⁴*Mechanical and Materials Engineering, University of Nebraska-Lincoln, Lincoln, Nebraska 68588, USA*

songyf_ut@163.com, kube@psu.edu, pzx@swu.edu.cn, jaturner@unl.edu; lixb_ex@163.com

Abstract: Ultrasound is a prominent nondestructive testing modality for the detection, localization, and sizing of defects in engineering materials. Often, inspectors analyze ultrasonic waveforms to determine if echoes, which stem from the scattering of ultrasound from a defect, exceed a threshold value. In turn, the initial selection of the threshold value is critical. In this letter, a time-dependent threshold or upper bound for the signal envelope is developed based on the statistics governing the scattering of ultrasound from microstructure. The utility of the time-dependent threshold is demonstrated using experiments conducted on sub-wavelength artificial defects. The results are shown to enhance current nondestructive inspection practices.

© 2019 Acoustical Society of America

[CCC]

Date Received: December 11, 2018 **Date Accepted:** January 22, 2019

1. Introduction

The ultrasonic waveform observed when attempting to detect flaws in engineering materials often exhibits grain noise from the interaction of the wave field with the microstructure. In the pulse-echo configuration, the grain noise created by the microstructural interaction is also called the diffuse ultrasonic backscatter because of the lack of coherence of these signals with the incident wave. When a discontinuity such as void, inclusion, or crack is in the field of view of the transducer, the reflection can be masked by this noise, especially when the discontinuity has characteristic dimensions or morphology which is not distinct from the microstructure. Thus, the grain noise for a given material is often the dominant factor limiting the detection of defects and flaws.^{1,2}

Recently, Song *et al.* developed a mathematical formalism that incorporated the inherent material-dependent backscatter response into a protocol for identification of flaw echoes when backscatter is significant.³⁻⁵ The formalism, based on statistical extreme value theory, provides an explicit expression for the upper bound of maximum amplitudes of grain noise, which can be used as a time-dependent threshold to separate sub-wavelength micro-flaws from the background of grain noise under ultra-high gain. However, previous research was aimed at either the radio frequency (RF) signal³ and the absolute value (ABS) of the signal.^{4,5}

Ultrasonic inspection based on the amplitude of the signal envelope is popular among inspectors because of its straightforward interpretation. Moreover, Thompson and Margetan indicated that the noise envelope distribution plays a fundamental role in the prediction of the probability of detection (POD), a key parameter used to manage the life of structural parts such as aircraft engines.⁶ The POD is also associated with the smallest detectable flaw size, which restricts the load capacities of damage tolerance design and lightweight design for structural parts. Considering a process in which a noise free flaw echo and grain noise add linearly, and assuming normally distributed noise with envelope detection, the resulting distribution has been proven to follow the Rician distribution. Thus, the POD value for a specific threshold can be defined for the Rician distribution.^{6,7} Meanwhile, the probability of false alarms (PFAs) of the ultrasonic system should be kept as low as possible. However, in most cases these methods use relatively low gain and fixed threshold, such that they are not

^{a)} Author to whom correspondence should be addressed.

practical for detection of sub-wavelength micro-flaws. To determine the smallest detectable flaw size under ultra-high gain using POD and PFA models, the noise envelope distribution and the relevant time-dependent threshold need to be derived.

In this letter, the enhanced ultrasonic flaw detection method is expanded to include the backscatter signal envelope, which is assumed to obey a Rayleigh distribution. This assumption allows the max-domain of attraction of the Rayleigh distribution to be determined. Then, we give and proof the normalizing constants of the asymptotic distribution of the largest order statistic from the Rayleigh distribution. Thus, the theoretical upper bound of the backscatter signal envelope can be given by the normalizing constants and the diffuse backscatter model from Turner and co-workers.⁸⁻¹⁰ Finally, the present method is verified using scattering measurements performed on a stainless steel specimen with artificial flat bottom holes (FBHs) designed with sub-wavelength dimensions.

2. Theory and method

Let the total number of ultrasonic signal envelopes acquired in an experiment be N . The i th ultrasonic waveform in the ensemble is a backscatter signal envelope denoted as $E_i(t)$, whose corresponding RF signal is denoted as $V_i(t)$. Suppose that $V_i(t)$ belongs to a normal distribution with zero-mean and standard deviation $\Sigma(t)$, such that $E_i(t)$ is a member of the Rayleigh distribution. If all the waveforms are independent and identically distributed (IID), the experimental maximum amplitudes in the ensemble are

$$A_{\max}^{\text{exp}}(t) = \max [E_i(t)]. \tag{1}$$

The goal of this letter is to build the theoretical maximum amplitudes $A_{\max}^{\text{theory}}(t)$ and their bounds for signal envelopes. The superscripts exp and theory are used to indicate the experimental and the theoretical quantities, respectively.

The probability density function (PDF) and the cumulative distribution function (CDF) of $E_i(t)$ are given, respectively, by

$$f[E(t)] = \frac{E(t)}{[\Sigma(t)]^2} \exp \left[-\frac{E(t)^2}{2[\Sigma(t)]^2} \right], \tag{2}$$

$$F[E(t)] = \int_0^{E(t)} f(Z) dZ = 1 - \exp \left[-\frac{E(t)^2}{2[\Sigma(t)]^2} \right], \tag{3}$$

where $i = 1, 2, \dots, N$ and $E(t) > 0$. As shown in [Appendix A](#), the Rayleigh CDF, F , belongs to the max-domain of attraction of the Gumbel extreme value distribution, with normalized constants $a_N(t) = \Sigma(t)/\sqrt{2\ln N}$ and $b_N(t) = \Sigma(t)\sqrt{2\ln N}$. Then, the mathematical expectation and the confidence bound of $A_{\max}^{\text{theory}}(t)$ can be given according to the properties of the Gumbel distribution. The mathematical expectation of $A_{\max}^{\text{theory}}(t)$ for the backscatter signal envelope is then¹¹

$$A_{\max}^{\text{theory}}(t) = b_N(t) + a_N(t)\gamma = \frac{(\gamma + 2\ln N)}{\sqrt{2\ln N}} \Sigma^{\text{theory}}(t), \tag{4}$$

where $\gamma \approx 0.5772$ is the Euler–Mascheroni constant and $\Sigma^{\text{theory}}(t)$ is the theoretical spatial standard deviation curve. The upper bound of $A_{\max}^{\text{theory}}(t)$ can be approximated as $U_1^{\text{theory}}(t) = b_N(t) - a_N(t)\ln[-\ln(\alpha)]$.¹¹ However, this approximate expression is based on the asymptotic behavior of the Gumbel distribution, which requires $N \rightarrow \infty$. Alternatively, we derive $U_2^{\text{theory}}(t)$ in [Appendix A](#) as

$$U_2^{\text{theory}}(t) = \Sigma^{\text{theory}}(t)\sqrt{2[\ln N - \ln(N - N\alpha^{1/N})]}, \tag{5}$$

where α is the confidence level. Equation (5) is the primary result of this letter. The difference between $U_1^{\text{theory}}(t)$ and $U_2^{\text{theory}}(t)$ is discussed in [Sec. 3](#).

Finally, $\Sigma^{\text{theory}}(t)$ can be estimated by the diffuse backscatter model that has been developed previously^{4,5} for which

$$\Sigma^{\text{theory}}(t) = \sqrt{\Phi^0 \tilde{\eta} \Xi \dots \psi(t)}, \tag{6}$$

where Φ^0 is the system calibration coefficient. In [Eq. \(6\)](#), $\tilde{\eta}$ and $\Xi \dots$ represent geometric and elastic properties of the microstructure and are defined as the spatial Fourier transform of the two-point correlation function, and the inner product between wave vectors and eighth-rank covariance tensor of the elastic moduli, respectively.¹² $\psi(t)$ is a temporal and spatial integration related to the transducer beam pattern. Explicit parameter definitions are dependent on the specific experimental case.⁸⁻¹⁰ In

practice, the upper bound $U_1^{\text{theory}}(t)$ or $U_2^{\text{theory}}(t)$ can be used to establish a time-dependent threshold to be triggered by an echo caused by a flaw.⁵ In addition, the lower bound can be calculated by an analogous form to Eq. (5). However, it is beyond the scope of the present letter.

3. Experiments and results

The flaw detection experiments are performed on a 304 stainless steel specimen. It has a ϕ 0.3 mm FBH with 10 mm depth, and two ϕ 0.2 mm FBHs with 10 and 12 mm depths, respectively; besides the FBH region, it has a reference region which is assumed free of any flaws (see Fig. 2 in Ref. 5) and is used to quantify the grain noise. The thickness of the specimen is 15 mm. The mean grain diameter is $44.2 \pm 2.8 \mu\text{m}$ revealed by optical microscopy via ASTM standard E112.¹⁵

The C-scan immersion system employs a JSR DPR-300 pulser/receiver (Pittsford, NY), an Olympus 7.5 MHz focused transducer (Waltham, MA, 51.9 mm focal length, 12.7 mm element diameter), a 200 MHz ADLink PCIe-9852 DAQ card (Beijing, China), and a computer-controlled motion platform. Normal incidence pulse/echo measurements are used. The spot size of this focused transducer is ~ 3.2 mm (much larger than the mean grain diameter of $44.2 \mu\text{m}$), which means the backscatter signal envelopes are expected to have a Rayleigh distribution. The couplant is water, whose density, longitudinal wave velocity, and attenuation coefficient are $\rho_f = 998 \text{ kg/m}^3$, $c_f = 1486 \text{ m/s}$, and $\alpha_f = 1.42 \text{ Np/m}$, respectively. The single crystal elastic constants of the stainless steel are assumed to be $c_{11} = 204.6 \text{ GPa}$, $c_{12} = 137.7 \text{ GPa}$, $c_{44} = 126.2 \text{ GPa}$.⁵ Its density, longitudinal wave velocity, and attenuation coefficient are measured as $c_L = 5855 \text{ m/s}$ and $\alpha_L = 8.76 \text{ Np/m}$ at 7.5 MHz. The focus is set in the middle of the specimen, i.e., the material path is 7.50 mm, such that the water path is $z_f = 22.4 \text{ mm}$.

To enhance the sensitivity of flaw detection, an ultra-high gain of 57 dB is used. Before scanning the FBH region, we need to verify the accuracy of the mathematical expectation, Eq. (4), and the upper bound, Eq. (5), for the maximum amplitude curve. Thus, the microstructure reference region, which is assumed to be free of flaws, is scanned with a resolution of 0.4 mm, and 900 waveforms are recorded. The corresponding spatial correlation coefficient (SCC) is checked as 0.46 ± 0.11 to meet the IID condition with a time gate from 32.0 to $34.5 \mu\text{s}$. Note that the SCC needs another independent test with RF signals due to the original definition of SCC in Ref. 13. Using the known mean grain diameter as input, the theoretical maximum amplitudes of the signal envelopes, the bounds, and the experimental result are shown in Fig. 1. It should be noted that $A_{\text{max}}^{\text{theory}}(t)$ mainly agrees with $A_{\text{max}}^{\text{exp}}(t)$, but $A_{\text{max}}^{\text{theory}}(t)$ is slightly larger at the peak. The reason may be that the asymptotic Gumbel distribution needs $N \rightarrow \infty$. Nevertheless, the mathematical expectation will not be used to detect flaws. The upper bounds agree well with the experimental result. The actual probabilities that $A_{\text{max}}^{\text{exp}}(t)$ lies below these two types of 95% upper bounds are 100% and 98.8% via the above-mentioned time gate. Thus, $U_2^{\text{theory}}(t)$ works better than $U_1^{\text{theory}}(t)$, and its error might be due to the non-Rayleigh distribution of the data. Moreover, the deviations at late arrival times are attributed to the limitations of the single scattering

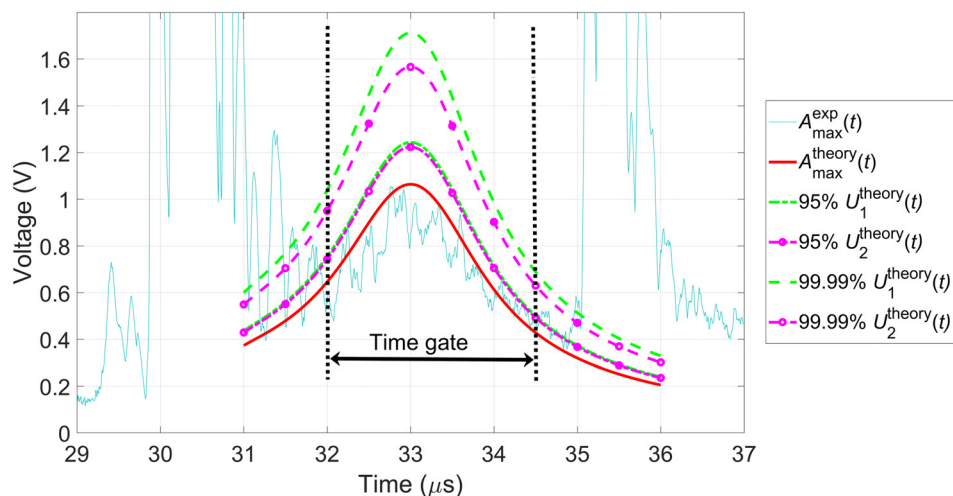


Fig. 1. (Color online) The maximum amplitudes of enveloped backscattering signals and the effects of confidence level on two kinds of upper bounds.

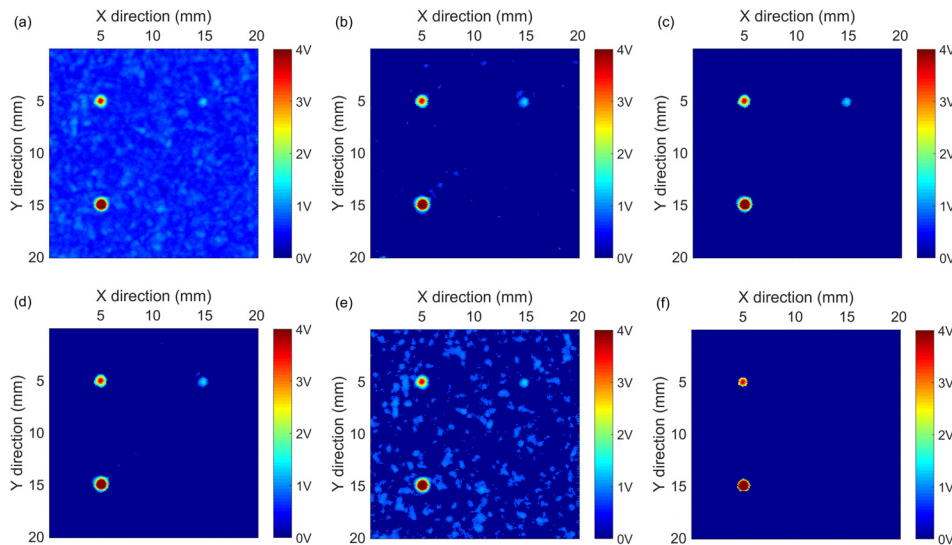


Fig. 2. (Color online) The C-scan images of the FBHs after image segmentation. (a) Raw C-scan, (b) time-dependent threshold for the signal envelope with $\alpha = 95\%$, (c) time-dependent threshold for the signal envelope with $\alpha = 99.99\%$, (d) time-dependent threshold for ABS signal with $\alpha = 99.99\%$, (e) fixed threshold 0.7 V, and (f) fixed threshold 1.4 V.

assumption. Fortunately, a higher confidence level can guarantee all the grain noise is captured. Therefore, we use $U_2^{\text{theory}}(t)$ with a 99.99% confidence level as the time-dependent threshold for flaw detection.

Next, the artificial FBH region that includes the micro-flaws is scanned with a resolution of 0.4 mm. Figure 2 shows the C-scan images of the FBHs before and after image segmentation using different thresholds. It still has some false positives when using an upper bound of 95% as Fig. 2(b) shows. However, all of these three micro-flaws are clearly visible in Fig. 2(c) when the 99.99% upper bound is used. For comparison, the 99.99% upper bound for the ABS signal described in Ref. 5 is used to generate Fig. 2(d), and a few false positives appear. Moreover, fixed thresholds using 0.7 and 1.4 V are applied in Figs. 2(e) and 2(f). False positives and missed detections result as expected. The deeper ϕ 0.2 mm FBH is missed completely in Fig. 2(f).

To further illustrate the present method, Fig. 3 shows the relationship between the flaw echo of the deeper ϕ 0.2 mm FBH, and the grain noise, the theoretical upper bound $U_2^{\text{theory}}(t)$ with 99.99% confidence level, and the fixed threshold of 1.4 V. Compared with Fig. 6 in Ref. 5, the signal envelopes are more succinct, but the performance based on the signal envelope is as good as that based on the ABS signals previously. More importantly, a 15 MHz transducer was used previously,⁵ but here a 7.5 MHz transducer is used. Thus, the ϕ 0.2 mm FBHs are only 0.256λ here, and the flaws smaller than 0.5λ were hard to detect before.

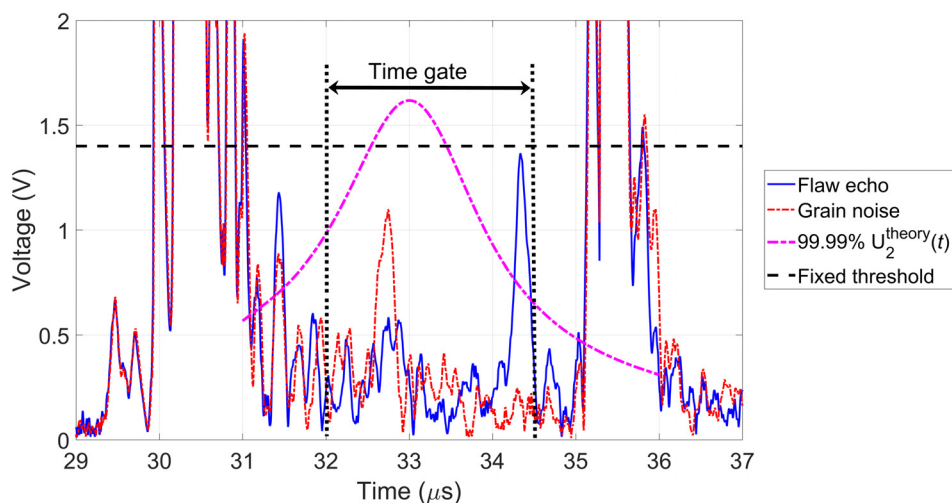


Fig. 3. (Color online) The relationship between the waveforms, the thresholds, and the time gate. The flaw echo based on the envelope is from a ϕ 0.2 mm FBH with 12 mm depth.

It should be noted that the apparent dimensions of the detected micro-flaws in the C-scan image, as seen in Fig. 2, are larger than the actual size. The reason for the larger apparent size is in the spreading of the scattered field from the sub-wavelength flaw.¹⁴ A secondary “blurring” effect caused by the interaction between the grain and flaw scattering could also be present. Both of these effects will exhibit an inherent depth dependence, which indicate the inadequacy of a fixed threshold and promotes our use of a depth- or time-dependent threshold.

Additionally, it is worthwhile to emphasize that our original interest for this work is the prediction of the POD, the PFA, and the smallest detectable flaw size. In terms of the calculation scheme of the physics-based POD and PFA models from Thompson and Margetan (see Fig. 11 in Ref. 6), the Gumbel distribution given in this letter is introduced to improve the threshold selection method as shown in Fig. 4. The diffuse ultrasonic scattering model⁸⁻¹⁰ and the ultrasonic measurement model¹⁴ are the cores of the physics-based POD and PFA models. The four models that appear in the upper-most portion of the figure represent the input factors. The instantaneous noise envelope distribution, maximum noise distribution, and distribution of the coherent

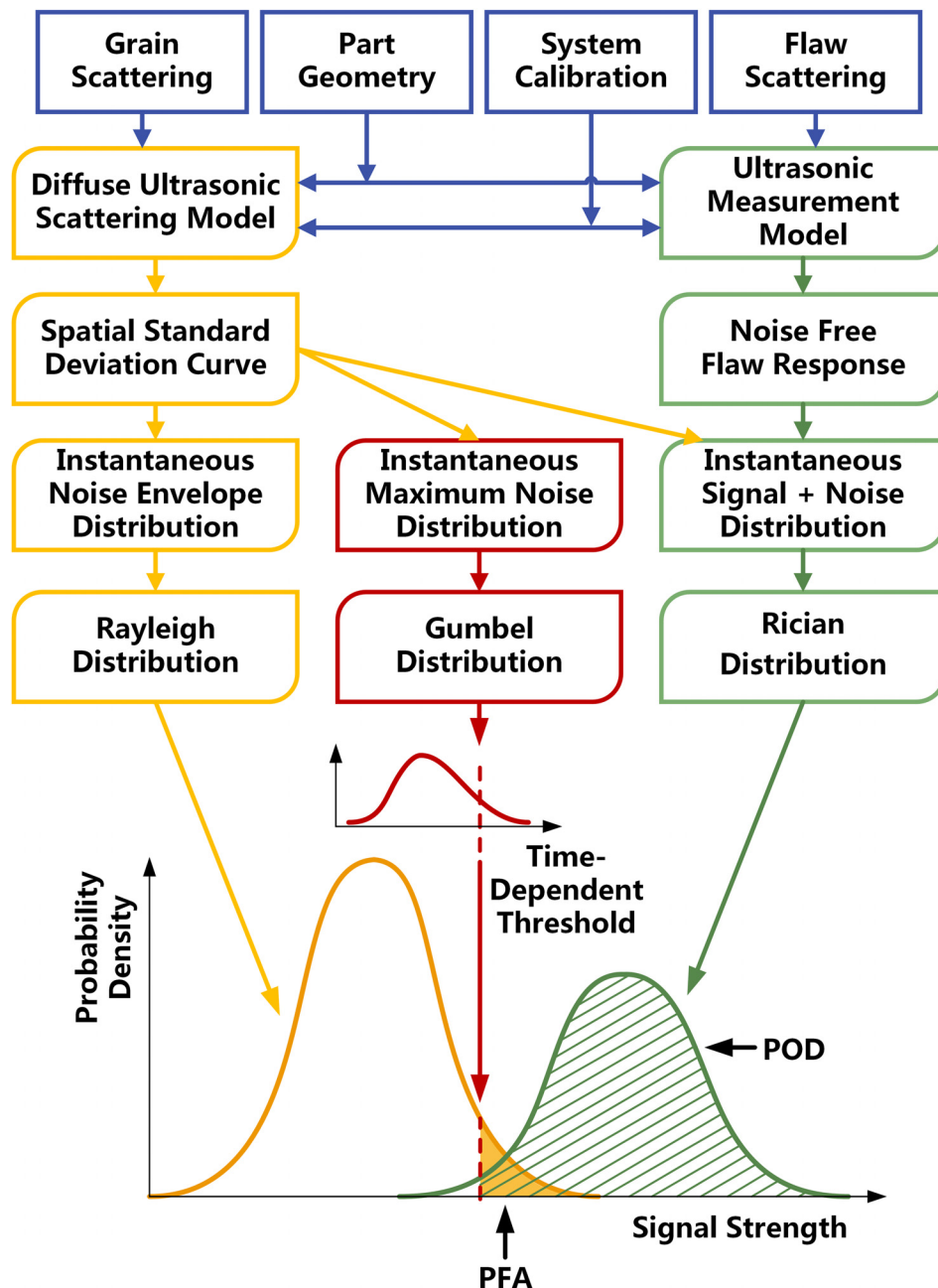


Fig. 4. (Color online) Schematic diagram showing the role played by the Rayleigh, Gumbel, and Rician distributions in determining POD and PFA.

superposition of signal and noise then can be deduced by the spatial standard deviation curve and the noise free flaw response. They can be described by the Rayleigh, Gumbel, and Rician distributions, respectively. In the end, we can determine the POD and PFA values at specific time points, i.e., the time-dependent POD and PFA models. Although this work itself seems like a parallel development to our previous works, the authors believe that the results can be used to build physics-based POD and PFA models in the near future.

4. Conclusion

In this article, upper bounds to the amplitude of ultrasonic backscatter signal envelopes were established based on extreme value distributions. The mathematical expectation and confidence estimate to the upper bound are given when the scattered signals can be assumed to belong to a Rayleigh distribution. In conjunction with experimental measurements, the model demonstrates the ability to detect internal micro-flaws that are $-\lambda/4$ dimension in a fine-grained stainless steel specimen. In combination with previous works, the enhanced ultrasonic flaw detection method has been verified universally for several signal types, including RF, ABS, and signal envelope. In the future, a model-assisted POD model based on the present technique will be explored to aid in the detection, localization, and sizing of a micro-flaw.

Acknowledgments

This work was supported by the National Natural Science Foundation of China (Grant Nos. 51575541 and 51711530231).

APPENDIX A

Brief proofs are given here for the propositions that the Rayleigh distribution belongs to the max-domain of attraction of the Gumbel extreme value distribution, and the normalized constants are $a_N(t) = \Sigma(t)/\sqrt{2\ln N}$ and $b_N(t) = \Sigma(t)\sqrt{2\ln N}$. In the following, the superscripts exp and theory are ignored; also, the t dependence of $A_{\max}(t)$, $E_i(t)$, and $V_i(t)$ is suppressed for brevity, until it is necessary. The derivative of the PDF of the Rayleigh distribution is

$$f'(E) = \frac{df(E)}{dE} = \frac{1}{\Sigma^2} \left(1 - \frac{E^2}{\Sigma^2}\right) \exp\left(-\frac{E^2}{2\Sigma^2}\right). \tag{A1}$$

Then, we have

$$\frac{f'(E)[1 - F(E)]}{[f(E)]^2} = \frac{\Sigma^2}{E^2} - 1 \rightarrow -1, \quad E \rightarrow \infty. \tag{A2}$$

Thus, the Rayleigh CDF F belongs to the max-domain of attraction of the Gumbel extreme value distribution $\Lambda(E) = \exp[-\exp(-E)]$, following Proposition 1.1(b) of Resnick.¹¹

The remaining task is to find the normalized constants a_N and b_N , which lead to $\lim_{N \rightarrow \infty} \Pr\{A_{\max} \leq a_N E + b_N\} = \Lambda(E)$. Assume that $a_N = \Sigma/\sqrt{2\ln N}$ and $b_N = \Sigma\sqrt{2\ln N}$, such that

$$\begin{aligned} \Pr\{A_{\max} \leq a_N E + b_N\} &= [F(a_N E + b_N)]^N \\ &= \left[1 - \frac{1}{N} \exp\left(-E - \frac{E^2}{4\ln N}\right)\right]^N. \end{aligned} \tag{A3}$$

Because for large N , we have

$$\begin{aligned} &\exp\left\{N \ln \left[1 - \frac{1}{N} \exp\left(-E - \frac{E^2}{4\ln N}\right)\right]\right\} \\ &= \exp\left\{-\exp(-E) \left[1 - \frac{E^2}{4\ln N} + \frac{E^4}{32(\ln N)^2} + o((\ln N)^{-2})\right]\right\}. \end{aligned} \tag{A4}$$

Thus, Eq. (A3) can be rewritten as

$$\begin{aligned} \Pr\{A_{\max} \leq a_N E + b_N\} &= \left[1 - \frac{1}{N} \exp\left(-E - \frac{E^2}{4\ln N}\right)\right]^N \\ &\rightarrow \exp(-\exp(-E)), \end{aligned} \tag{A5}$$

as $N \rightarrow \infty$. Hence, the assumptions for the normalized constants a_N and b_N are correct.

Table 1. Normalizing constants and time-dependent thresholds for different signal mode.

Signal Mode	Underlying Distribution	Normalizing Constants	Time-Dependent Threshold
RF	Normal	$a_N = \Sigma/\sqrt{2\ln N},$ $b_N = \Sigma\left(\sqrt{2\ln N} - \frac{\ln\ln N + \ln 4\pi}{\sqrt{2\ln N}}\right)$	$U = b_N - a_N \ln[-\ln((1 + \alpha)/2)],$ $L = -b_N + a_N \ln[-\ln((1 + \alpha)/2)]$
ABS	Half normal	$a_N = \Sigma/\sqrt{2\ln N},$ $b_N = \Sigma\left(\sqrt{2\ln N} - \frac{\ln\ln N + \ln\pi}{\sqrt{2\ln N}}\right)$	$U = b_N - a_N \ln[-\ln(\alpha)]$
Enveloped	Rayleigh	$a_N = \Sigma/\sqrt{2\ln N},$ $b_N = \Sigma\sqrt{2\ln N}$	$U = b_N - a_N \ln[-\ln(\alpha)] \text{ or}$ $U = b_N + a_N H^{-1}(\alpha) \text{ with}$ $H(\alpha) = \left[1 - \frac{1}{N} \exp\left(-E - \frac{E^2}{4\ln N}\right)\right]^N$

Finally, to calculate the upper bound more accurately, we utilize the inverse solution of $H(\alpha) = \{1 - \exp[-E - E^2/(4\ln N)]/N\}^N$ to calculate the upper bound as

$$\begin{aligned}
 U_2(t) &= b_N(t) + a_N(t)H^{-1}(\alpha) \\
 &= \Sigma(t)\sqrt{2[\ln N - \ln(N - N\alpha^{1/N})]}. \tag{A6}
 \end{aligned}$$

APPENDIX B

A short summary and comparison of the extreme value distributions for different kinds of signals is given. The extreme value distribution of the RF signal, ABS signal, and signal envelope all follow the Gumbel distribution. As shown in Table 1, the only difference is the normalizing constant b_N . Considering the role of b_N on the upper bound, or the time-dependent threshold in the present method, if b_N gets larger, the time-dependent threshold becomes greater. Thus, the time-dependent threshold of the RF signal is seen to be the lowest while the threshold of the enveloped signal is the highest. Physically, this can be traced to the enveloped signal always being equal to or greater than the ABS signal.

References and links

- ¹R. B. Thompson and F. J. Margetan, "Ultrasonic scattering in polycrystals with orientation clusters of orthorhombic crystallites," *Wave Motion* **36**, 347–365 (2002).
- ²L. Moreau, A. J. Hunter, A. Velichko, and P. D. Wilcox, "3-D reconstruction of sub-wavelength scatterers from the measurement of scattered fields in elastic waveguides," *IEEE Trans. Ultrason. Ferroelec. Freq. Control* **61**, 1864–1879 (2014).
- ³Y. Song, X. Zi, Y. Fu, X. Li, C. Chen, and K. Zhou, "Nondestructive testing of additively manufactured material based on ultrasonic scattering measurement," *Measurement* **118**, 105–112 (2018).
- ⁴Y. Song, C. M. Kube, J. A. Turner, and X. Li, "Statistics associated with the scattering of ultrasound from microstructure," *Ultrasonics* **80**, 58–61 (2017).
- ⁵Y. Song, J. A. Turner, Z. Peng, C. Chao, and X. Li, "Enhanced ultrasonic flaw detection using an ultra-high gain and time-dependent threshold," *IEEE Trans. Ultrason. Ferroelec. Freq. Control* **65**, 1214–1225 (2018).
- ⁶R. B. Thompson and F. J. Margetan, "Use of elastodynamic theories in the stochastic description of the effects of microstructure on ultrasonic flaw and noise signals," *Wave Motion* **36**, 347–365 (2002).
- ⁷I. Yalda, F. J. Margetan, and R. B. Thompson, "Use of Rician distributions to predict the distributions of ultrasonic flaw signals in the presence of backscattered noise," in *Review of Progress in Quantitative NDE*, edited by D. O. Thompson and D. E. Chimenti (Plenum, New York, 1998), Vol. 17, pp. 105–112.
- ⁸G. Ghoshal and J. A. Turner, "Diffuse ultrasonic backscatter at normal incidence through a curved interface," *J. Acoust. Soc. Am.* **128**, 3449–3458 (2010).
- ⁹A. P. Arguelles, C. M. Kube, P. Hu, and J. A. Turner, "Mode-converted ultrasonic scattering in polycrystals with elongated grains," *J. Acoust. Soc. Am.* **140**, 1570–1580 (2016).
- ¹⁰P. Hu and J. A. Turner, "Transverse-to-transverse diffuse ultrasonic scattering," *J. Acoust. Soc. Am.* **142**, 1112–1120 (2017).
- ¹¹S. I. Resnick, *Extreme Values, Regular Variation and Point Processes* (Springer, New York, 1987), 320 pp.
- ¹²J. A. Turner and R. L. Weaver, "Radiative transfer and multiple scattering of diffuse ultrasound in polycrystalline media," *J. Acoust. Soc. Am.* **94**, 3675–3683 (1994).
- ¹³L. Yu, R. B. Thompson, and F. J. Margetan, "The spatial correlation of backscattered ultrasonic grain noise: Theory and experimental validation," *IEEE Trans. Ultrason. Ferroelec. Freq. Control* **57**, 1096–1111 (2010).
- ¹⁴L. W. Schmerr and S. J. Song, *Ultrasonic Nondestructive Evaluation System* (Springer, New York, 2007), Chap. 10.
- ¹⁵ASTM E112-13: *Standard Test Methods for Determining Average Grain Size* (ASTM International, Conshohocken, PA, 2013).